JOURNAL OF SPACECRAFT AND ROCKETS
Vol. 44, No. 6, November–December 2007

Tradeoff Performance of Hybrid Low-Thrust Propulsion System

Giovanni Mengali* and Alessandro A. Quarta†
University of Pisa, 56122 Pisa, Italy

DOI: 10.2514/1.30298

The employment of low-thrust propulsion systems is an attractive option for space missions requiring large changes in orbital energy. Therefore in this paper, we investigate the performance of a hybrid low-thrust propulsion system, constituted by a solar electric thruster coupled with a solar sail. Loosely speaking, the solar sail may be seen as a propellantless auxiliary system capable of reducing the gravitational force acting on the spacecraft in such a way that the propellant expense for a given mission may be decreased. To quantify this effect, we analyze the problem in terms of optimization of a scalar performance index that takes into account both the mission time and the propellant mass required to reach the target orbit. A weighting parameter is used to trade between these two conflicting requirements. The problem is solved using an indirect approach and the resulting optimal control law is applied to a circle-to-circle rendezvous transfer. Key features of the paper are the use of realistic models for both the solar electric thruster and the solar sail.

Nomenclature

A	=	sail area
a	=	spacecraft acceleration
a_c	=	sail characteristic acceleration
b_1, b_2, b_3	=	force coefficients
f_i, g_i	=	constant coefficients
H	=	Hamiltonian
H'	=	Hamiltonian that explicitly depends on the control vector
h	=	performance parameter
J	=	performance index
k	=	switching function
m	=	spacecraft mass
$\boldsymbol{n}$	=	sail normal vector
P	=	electric thruster input power
$P_\odot$	=	solar radiation pressure
$\boldsymbol{r}$	=	sun-spacecraft position vector, $r \triangleq \|\boldsymbol{r}\|$
$\boldsymbol{T}$	=	electric propulsion system thrust
t	=	time
$\boldsymbol{u}$	=	control vector
u	=	radial velocity
v	=	circumferential velocity
α	=	sail pitch angle
α_λ	=	primer vector pitch angle
β_σ	=	dimensionless sail loading
η	=	tradeoff parameter
θ	=	polar angle
λ	=	adjoint variable
$\mu_\odot$	=	sun's gravitational parameter
σ	=	sail loading
σ_{SS}	=	sail assembly loading
τ	=	electric thruster switching parameter
φ	=	thrust angle

Subscripts

e	=	solar electric propulsion system
f	=	final
m	=	pertaining to the mass
p	=	propellant
pay	=	payload
r	=	radial
u	=	pertaining to the radial velocity
v	=	pertaining to the circumferential velocity
θ	=	circumferential
0	=	initial
$\oplus$	=	Earth
$\male$	=	Mars
$\female$	=	Venus

Superscripts

$\dot{}$	=	time derivative
$\hat{}$	=	unit vector
$\tilde{}$	=	optimal
$\star$	=	reference value

Introduction

A NUMBER of space transportation systems have been developed for solar system exploration to deepen our knowledge of the formation and evolution of the planetary environment [1–7]. To reduce the mission costs or enable missions that cannot currently be accomplished, significant efforts are necessary for the development of advanced technologies. These include substantial testing of new approaches, systems, and operations as well as the coordination of robotic elements along with human and cargo transportation systems over the next few decades or more [8–10].

The technology of advanced space propulsion is important especially due to the challenges of performing complex trajectories. In this context, the employment of low-thrust propulsion systems becomes a primary option, especially for those missions requiring large changes in orbital energy. Although solar electric propulsion (SEP) may be seen as the most natural propulsion means, other possibilities can be exploited. In particular, the idea of combining an SEP with an auxiliary system constituted by a solar sail to obtain a hybrid low-thrust propulsion (HLTP) system, has been recently proposed by Mengali and Quarta [11] and discussed under simplified assumptions. In [11], the SEP system is assumed to supply a constant thrust whose steering law is the output of an optimization process

Received 6 February 2007; revision received 20 April 2007; accepted for publication 28 April 2007.

*Associate Professor, Department of Aerospace Engineering; g.mengali@ing.unipi.it. Member AIAA.

†Research Assistant, Department of Aerospace Engineering; a.quarta@ing.unipi.it. Member AIAA.

aiming to maximize the spacecraft mass at the final mission time. Also, the solar sail is described through a nonperfect reflection model and is assumed to be capable of providing an inverse square pure radial thrust. As a result, the spacecraft "senses" a gravitational force whose magnitude is reduced with respect to the local solar gravity. Exploiting the size of the reduction of the gravitational acceleration as a control parameter, an increase of that parameter provides better performance both in terms of propellant consumption saving and decrease of mission time in the examples considered [11].

The aim of this paper is to extend the results of [11] and refine the mathematical model employed therein in several ways. First, the solar sail thrust is now controlled via the sail pitch angle and is assumed to be independent of the SEP control parameters. Second, the SEP system is more accurately modeled, through a second-order polynomial approximation for the thrust and the propellant mass flow rate as a function of the thruster input power. Finally, the HLTP performance is investigated by optimizing a scalar performance index that contains a weighted sum of the total mission time and the propellant mass required to reach the mission target. The solution of such an optimization process allows one to perform tradeoff studies between minimum-time trajectories and minimum propellant transfers, and to fully exploit the potential of HLTP for future missions.

Equations of Motion

Consider a spacecraft with an HLTP system in which an SEP system is coupled with a flat solar sail (SS). The corresponding total spacecraft acceleration is given by the sum of two terms representing the contribution of the two propulsion systems alone, that is

$$\boldsymbol{a} = \boldsymbol{a}_{\mathrm{SEP}} + \boldsymbol{a}_{\mathrm{SS}} \tag{1}$$

The heliocentric equations of motion for a spacecraft of total mass m in a polar inertial frame $\mathcal{T}$ are

$$\dot{r} = u \tag{2}$$

$$\dot{\theta} = \frac{v}{r} \tag{3}$$

$$\dot{u} = \frac{v^2}{r} - \frac{\mu_\odot}{r^2} + a_r \tag{4}$$

$$\dot{v} = -\frac{uv}{r} + a_\theta \tag{5}$$

$$\dot{m} = -\dot{m}_p \tag{6}$$

where θ is measured counterclockwise from some reference position.

Solar Electric Propulsion Mathematical Model

In this paper, we assume that the SEP system performance, in terms of available thrust $\boldsymbol{T}$ and propellant mass flow rate $\dot{m}_p$, are a function of the total electric thruster input power P which is supplied to the thruster by the power processing unit. Both the thrust and the propellant mass flow rate depend on P, where P, by assumption, is a control variable that can be continuously adjusted in the range $P \in [P_{\min}, P_{\max}]$. The endpoints of the power variation interval depend on the thruster operational characteristics. The assumption concerning the continuity of P approximates the actual thruster behavior which allows the input power to be set at a finite, albeit large, number of operating points (usually on the order of 100).

The boundary values of P are $P_{\min} = 0.46$ kW and $P_{\max} = 1.5$ kW. Note that the switching parameter $\tau = (0, 1)$ models the thruster on/off condition and allows one to account for coasting arcs in the spacecraft trajectory. The components of $\hat{\boldsymbol{T}}$ in the polar frame are

$$[\hat{\boldsymbol{T}}]_{\mathcal{T}} = [\cos\varphi, \sin\varphi]^T \tag{7}$$

where the thrust angle $\varphi \in [0, 2\pi]$ is measured counterclockwise from the radial direction.

The relationships $\boldsymbol{T} = \boldsymbol{T}(P)$ and $\dot{m}_p = \dot{m}_p(P)$ are obtained through a best-fit of experimental data and are expressed using a suitable polynomial approximation. For a preliminary mission analysis, a second-order polynomial approximation is adequate, that is [12]

$$\boldsymbol{T} = (f_2 P^2 + f_1 P + f_0)\tau \hat{\boldsymbol{T}} \tag{8}$$

$$\dot{m}_p = (g_2 P^2 + g_1 P + g_0)\tau \tag{9}$$

where f_i and g_i (with $i = 0, 1, 2$) are constant coefficients. Table 1 shows the coefficients corresponding to the PPS-1350-G Hall-effect thruster, mounted on the ESA SMART-1 spacecraft [12,13].

From Eqs. (7) and (8), the radial and circumferential acceleration due to the SEP system are

$$a_{\mathrm{SEP}_r} = \tau \frac{f_2 P^2 + f_1 P + f_0}{m} \cos\varphi \tag{10}$$

$$a_{\mathrm{SEP}_\theta} = \tau \frac{f_2 P^2 + f_1 P + f_0}{m} \sin\varphi \tag{11}$$

Solar Sail Mathematical Model

Here we assume a flat solar sail with an optical force model [14,15]. The propulsive sail acceleration can be written as [16]

$$\boldsymbol{a}_{\mathrm{SS}} = \frac{P_\odot A}{m} \cos\alpha [b_1 \hat{\boldsymbol{r}} + (b_2 \cos\alpha + b_3)\hat{\boldsymbol{n}}] \tag{12}$$

where b_1, b_2, and b_3 are the force coefficients related to the thermooptical properties of the reflective film [14,16] and $\hat{\boldsymbol{n}}$ is in the direction $\hat{\boldsymbol{r}} \cdot \hat{\boldsymbol{n}} > 0$. The force coefficients, as usual, are assumed to be independent of the sail attitude and constant over the whole mission. For a highly reflective aluminum-coated front side and a highly emissive chromium-coated back side, one has [16] $b_1 = 0.1728$, $b_2 = 1.6544$, and $b_3 = -0.0109$. These values are used in all of the succeeding simulations.

In Eq. (12), the sail pitch angle $\alpha \in [-\pi/2, \pi/2]$ represents the sail control variable and is defined as

$$\cos\alpha = \hat{\boldsymbol{r}} \cdot \hat{\boldsymbol{n}} \tag{13}$$

From Eq. (12), the acceleration provided by the solar sail is independent of the SEP thrust control parameters, described by Eqs. (10) and (11). This is clearly a simplification, which is adopted for the sake of mathematical tractability. In practice, the situation could be more involved due to different reasons, such as, for example, the possible interference of the SEP exhaust plume with the sail reflecting surface. However, we will not pursue further these problems and refer the reader to consult the interesting report by Leipold and Götz [17].

As stated, the solar sail performance (in terms of thrust magnitude and direction) is assumed to be unaffected by the SEP performance, thus neglecting all kinds of coupling between the two propulsion systems. The expression for the sail acceleration, Eq. (12), can be more conveniently expressed with the introduction of the dimensionless sail loading parameter β_σ. The latter is defined [11] as $\beta_\sigma \triangleq \sigma^\star/\sigma$, where $\sigma^\star \triangleq 2P_\odot/(\mu_\odot/r_\oplus^2) = 1.539$ g/m^2 is a reference sail loading parameter, $r_\oplus = 1$ AU and $\sigma \triangleq m/A$ is a generalized sail loading. Note that both β_σ and σ vary with time because the total spacecraft mass decreases (when $\tau = 1$) according to Eq. (6) due to the propellant consumption. Let

$$\beta_{\sigma_0} \triangleq \frac{\sigma^\star}{m_0/A} \tag{14}$$

be the initial (given) dimensionless sail loading. Then

$$\beta_\sigma = \beta_{\sigma_0} \frac{m_0}{m} \tag{15}$$

Combining Eq. (14) with the definition of β_σ and σ^* yields

$$\frac{P_\odot A}{m} = \frac{\beta_{\sigma_0}\mu_\odot}{2r^2}\left(\frac{m_0}{m}\right) \tag{16}$$

Note that β_{σ_0} (or m_0/A) is a technological parameter, based on the limits of the current (or future) sail technology [18].

A relationship exists between the dimensionless sail loading and the characteristic acceleration a_c, the latter being the parameter commonly used to quantify the performance of a solar sail. If one thinks of a_c as the solar radiation pressure acceleration acting on an ideal solar sail (that is [16], a perfectly reflecting sail with $b_1 \equiv b_3 = 0$ and $b_2 = 2$) oriented perpendicular ($\alpha = 0$) to the sun line at $r = r_\oplus$, one has

$$a_c = \beta_\sigma \frac{\mu_\odot}{r_\oplus^2} \tag{17}$$

where $\mu_\odot/r_\oplus^2 \cong 5.930$ mm/s^2 is the sun's gravitational acceleration at 1 AU distance.

Substituting Eq. (15) into Eq. (12) and recalling Eq. (13), the radial a_{SS_r} and circumferential a_{SS_θ} sail acceleration components become

$$a_{\mathrm{SS}_r} = \frac{\beta_{\sigma_0}\mu_\odot}{2r^2}\left(\frac{m_0}{m}\right)\cos\alpha(b_1 + b_2\cos^2\alpha + b_3\cos\alpha) \tag{18}$$

$$a_{\mathrm{SS}_\theta} = \frac{\beta_{\sigma_0}\mu_\odot}{2r^2}\left(\frac{m_0}{m}\right)\sin\alpha\cos\alpha(b_2\cos\alpha + b_3) \tag{19}$$

Equations (10), (11), (18), and (19) allow one to calculate the expressions of the total radial and circumferential acceleration of the spacecraft as $a_r = a_{\mathrm{SEP}_r} + a_{\mathrm{SS}_r}$, and $a_r = a_{\mathrm{SEP}_\theta} + a_{\mathrm{SS}_\theta}$. Finally, note that $|\dot{m}| \equiv |\dot{m}_p|$, because the solar sail is not responsible for any spacecraft mass variation.

Problem Statement

Consider an interplanetary circle-to-circle transfer problem between an initial ($t_0 = 0$) orbit of radius $r(0) = r_\oplus$ and a target coplanar orbit of radius $r(t_f) = r_f$. The problem addressed here is that of finding the optimal control law that maximizes the performance index J defined as

$$J \triangleq \eta\frac{m_f}{m_0} - (1-\eta)\frac{t_f}{t^\star} \tag{20}$$

where the reference time $t^\star \triangleq 2\pi\sqrt{r_\oplus^3/\mu_\odot}$ is introduced to make J dimensionless and $\eta \in [0, 1]$ is a tradeoff parameter.

Note that J includes the two classical conflicting requirements of a spacecraft mission, that is, the total mission time t_f and the propellant mass required to reach the target orbit. The tradeoff parameter weighs the relative importance of these two requirements in the determination of the optimal trajectory. The boundary values for η correspond to the minimum-time trajectory $\eta = 0$ and to the minimum propellant rendezvous transfer $\eta = 1$.

Optimal Control Laws

In mathematical terms, we look for the control law $\boldsymbol{u}(t)$, where $\boldsymbol{u} \triangleq [P \quad \tau \quad \varphi \quad \alpha]^T$ is the control vector, which maximizes J through an indirect approach. From Eqs. (2–6), the Hamiltonian of the system is

$$H = \lambda_r u + \lambda_\theta\frac{v}{r} + \lambda_u\left(\frac{v^2}{r} - \frac{\mu_\odot}{r^2} + a_r\right) + \lambda_v\left(-\frac{uv}{r} + a_\theta\right) - \lambda_m\dot{m}_p \tag{21}$$

where λ_r, λ_θ, λ_u, λ_v, and λ_m are the adjoint variables associated with the state variables r, θ, u, v, and m, respectively. The time derivatives of the adjoint variables are provided by the Euler–Lagrange equations

$$\dot{\lambda}_r = \frac{\lambda_\theta v}{r^2} + \lambda_u\left(\frac{v^2}{r^2} - \frac{2\mu_\odot}{r^3} - \frac{\partial a_r}{\partial r}\right) - \lambda_v\left(\frac{uv}{r^2} + \frac{\partial a_\theta}{\partial r}\right) \tag{22}$$

$$\dot{\lambda}_\theta = 0 \tag{23}$$

$$\dot{\lambda}_u = -\lambda_r + \lambda_v\frac{v}{r} \tag{24}$$

$$\dot{\lambda}_v = -\frac{\lambda_\theta}{r} - 2\frac{\lambda_u v}{r} + \frac{\lambda_v u}{r} \tag{25}$$

$$\dot{\lambda}_m = \frac{\lambda_u a_r + \lambda_v a_\theta}{m} \tag{26}$$

From Pontryagin's maximum principle, the optimal control law $\boldsymbol{u}(t)$, to be selected in the domain of feasible controls $\mathcal{U}$, is such that, at any time, the Hamiltonian is an absolute maximum. This amounts to maximizing the function H' which coincides with that portion of the Hamiltonian H that explicitly depends on the control vector:

$$\boldsymbol{u} = \arg\max_{\boldsymbol{u}\in\mathcal{U}} H' \quad \text{with} \quad H' \triangleq \lambda_u a_r + \lambda_v a_\theta - \lambda_m\dot{m}_p \tag{27}$$

that is

$$\varphi(t) = \arg\max_{\eta\in[0,2\pi]}(\lambda_u\cos\varphi + \lambda_v\sin\varphi) \tag{28}$$

$$P(t) = \arg\max_{P\in[P_{\min},P_{\max}]}(q_2P^2 + q_1P + q_0) \tag{29}$$

$$\tau(t) = \arg\max_{\tau=(0,1)}(k\tau) \tag{30}$$

$$\alpha(t) = \arg\max_{\alpha\in[-\pi/2,\pi/2]}(\lambda_u a_{\mathrm{SS}_r} + \lambda_v a_{\mathrm{SS}_\theta}) \tag{31}$$

with

$$q_i \triangleq \frac{f_i(\lambda_u\cos\varphi + \lambda_v\sin\varphi)}{m} - g_i\lambda_m \qquad (i = 0, 1, 2) \tag{32}$$

$$k \triangleq \frac{f_2P^2 + f_1P + f_0}{m}(\lambda_u\cos\varphi + \lambda_v\sin\varphi) - \lambda_m(g_2P^2 + g_1P + g_0) \tag{33}$$

The optimal thrust angle of Eq. (28) is [19]

$$\cos\varphi = \frac{\lambda_u}{\sqrt{\lambda_u^2 + \lambda_v^2}} \tag{34}$$

$$\sin\varphi = \frac{\lambda_v}{\sqrt{\lambda_u^2 + \lambda_v^2}} \tag{35}$$

From Eq. (29), the optimal electric thruster input power is obtained as

$$P = \begin{cases} -\frac{q_1}{2q_2} & \text{if } q_2 < 0 \cap -\frac{q_1}{2q_2} \in [P_{\min}, P_{\max}] \\ P_{\min} & \text{if } q_2 < 0 \cap -\frac{q_1}{2q_2} < P_{\min} \\ P_{\max} & \text{if } q_2 < 0 \cap -\frac{q_1}{2q_2} > P_{\max} \\ P_{\max} & \text{if } q_2 > 0 \cap -\frac{q_1}{2q_2} < \frac{P_{\min}+P_{\max}}{2} \\ P_{\min} & \text{if } q_2 > 0 \cap -\frac{q_1}{2q_2} > \frac{P_{\min}+P_{\max}}{2} \end{cases} \tag{36}$$

where, with the aid of Eqs. (32), (34), and (35) one has

$$-\frac{q_1}{2q_2} = \frac{g_1 m \lambda_m - f_1\sqrt{\lambda_u^2+\lambda_v^2}}{2(f_2\sqrt{\lambda_u^2+\lambda_v^2} - g_2 m \lambda_m)} \tag{37}$$

The optimal value of τ is easily found by noting that Eq. (30) is linear in the control variable. Therefore, the following bang–bang control law is obtained

$$\tau = \begin{cases} 0 & \text{if } k \le 0 \\ 1 & \text{if } k > 0 \end{cases} \tag{38}$$

where the switching function k is calculated through Eq. (33), after having substituted here the values of φ and P from Eqs. (34–36).

Finally, the optimal sail pitch angle is the angle that, at any time, maximizes the projection of $\boldsymbol{a}_{SS}$ on the direction of the primer vector [20] $\boldsymbol{\lambda} \triangleq [\lambda_u, \lambda_v]^T$. Following [16], α is closely related to the value attained by the primer vector pitch angle α_λ. The latter is defined in such a way that

$$\cos\alpha_\lambda \triangleq \frac{\lambda_u}{\sqrt{\lambda_u^2+\lambda_v^2}} \tag{39}$$

where $\alpha_\lambda \in [0, \pi]$. It can be shown that the optimal steering law is

$$\alpha = \begin{cases} \text{sgn}(\lambda_v)\tilde{\alpha} & \text{if } \alpha_\lambda < \alpha_\lambda^\star \\ \text{sgn}(\lambda_v)(\pi/2) & \text{if } \alpha_\lambda \ge \alpha_\lambda^\star \end{cases} \tag{40}$$

where sgn represents the signum function and the angle $\tilde{\alpha} \in [0, \pi/2]$ is obtained invoking the necessary condition $\partial H/\partial\alpha = 0$. The result is given by the following nonlinear equation [16]:

$$\tan\alpha_\lambda = \frac{\sin\tilde{\alpha}(b_1 + 3b_2\cos^2\tilde{\alpha} + 2b_3\cos\tilde{\alpha})}{\cos^2\tilde{\alpha}(b_2\cos\tilde{\alpha}+b_3) - \sin^2\tilde{\alpha}(2b_2\cos\tilde{\alpha}+b_3)} \tag{41}$$

The reference angle $\alpha_\lambda^\star \in [0, \pi]$ in Eq. (40) is related to the value of the optical force coefficients according to Eq. (42)

$$\tan\alpha_\lambda^\star = -\frac{2b_1 + (b_2B^2)/2 + b_3B}{(b_2B/2+b_3)\sqrt{4-B^2}} \tag{42}$$

where

$$B \triangleq \frac{-b_1b_3 - 2b_2b_3 - \sqrt{b_1^2b_3^2 - 4b_2b_1b_3^2 + 4b_1b_2^3 + 8b_2^2b_1^2}}{b_2^2 + 2b_2b_1} \tag{43}$$

The reference angle $\alpha_\lambda^\star$ may be seen as the primer vector pitch angle beyond which the optimal control law requires the thrust to be set to zero [16]. Using the previous numerical values of force coefficients ($b_1 = 0.1728$, $b_2 = 1.6544$, and $b_3 = -0.0109$), the reference primer vector pitch angle is $\alpha_\lambda^\star \cong 2.5392$ rad and the expression in radians for $\tilde{\alpha}$ [see Eq. (41)] is best-fit approximated, with errors less than 1%, by means of a sixth-order polynomial in the form

$$\tilde{\alpha} \cong 0.008109\alpha_\lambda^6 - 0.0547\alpha_\lambda^5 + 0.1356\alpha_\lambda^4 - 0.1266\alpha_\lambda^3 + 0.08266\alpha_\lambda^2 + 0.3038\alpha_\lambda + 0.0008666 \quad \text{for } \alpha_\lambda \in [0, \alpha_\lambda^\star] \tag{44}$$

Boundary-Value Problem

The boundary-value problem associated to the variational problem is constituted by the equations of motion (2–6) and the Euler–Lagrange Eqs. (22–26). The corresponding 10 boundary conditions are connected to the spacecraft position, velocity, and mass at the initial and at the (open) final time

$$r(t_0) = r_\oplus, \qquad \theta(t_0) = 0, \qquad u(t_0) = 0$$
$$v(t_0) = \sqrt{\frac{\mu_\odot}{r_\oplus}}, \qquad m(t_0) = m_0 \tag{45}$$

$$r(t_f) = r_f, \qquad \lambda_\theta(t_f) = 0, \qquad u(t_f) = 0$$
$$v(t_f) = \sqrt{\frac{\mu_\odot}{r_f}}, \qquad \lambda_m(t_f) = \frac{\eta}{m_0} \tag{46}$$

The mission time is obtained by enforcing the transversality condition [21]

$$H(t_f) = (1-\eta)/t^\star \tag{47}$$

The two point boundary-value problem is solved by finding the initial value of the adjoint variables λ_r, λ_u, λ_v, λ_m, and of the final time t_f. In fact, from Eqs. (23) and (46), one has $\lambda_\theta \equiv 0$ for $t \in [t_0, t_f]$.

Numerical Simulations

The previously discussed control law has been used to study optimal rendezvous missions toward Mars ($r_f \equiv r_\mathrm{♂} = 1.5237$ AU) and Venus ($r_f \equiv r_\mathrm{♀} = 0.7233$ AU). A number of trajectories have been simulated with values of the initial mass ranging in the interval $m_0 \in [200, 1000]$ kg. The coefficients f_i and g_i in Eqs. (8) and (9) correspond to the PPS-1350-G Hall-effect thruster and are shown in Table 1, whereas the power P is assumed to range between $P_{\min} = 0.46$ kW and $P_{\max} = 1.5$ kW. The boundary-value problem associated with the variational problem has been solved through a hybrid numerical technique combining genetic algorithms (to obtain an estimate of the adjoint variables and of the final time), with gradient-based and direct methods to refine the solution [16].

Minimum-Time Trajectories

Minimum-time trajectories are obtained by maximizing $J = -t_f/t^\star$, which amounts to solving the previously discussed optimal control problem with the constraint $\eta = 0$ [see Eq. (20)]. Figures 1 and 2 show the simulation results, in terms of dimensionless propellant mass ($m_p/m_0 = 1 - m_f/m_0$) and flight time, for Earth–Mars and Earth–Venus missions, with values of the initial dimensionless sail loading parameter ranging in the interval $\beta_{\sigma_0} \in [0, 0.5]$. Note that the line characterized by $\beta_{\sigma_0} = 0$ corresponds to the employment of a pure SEP propulsion system ($\beta_{\sigma_0} = 0 \Rightarrow \boldsymbol{a}_{SS} \equiv 0$ over the whole trajectory). This line has some local minima that differ in terms of initial spacecraft mass and mission time. The presence of these local minima is in accordance with the results found by Alfano and Thorne [22] who showed that a transfer between circular orbits has a minimum cost when an integer number of revolutions is enforced. This result, found under the assumption of constant thrust, is consistent with our simulations

Table 1 Polynomial coefficients f_i and g_i for the PPS-1350-G Hall-effect thruster (adapted from [12])

Coefficient	Value
f_0	4.68 mN
f_1	60.94 mN/kW
f_2	−5.1 mN/kW^2
g_0	1.935 mg
g_1	2.545 mg/kW
g_2	−0.3716 mg/kW^2

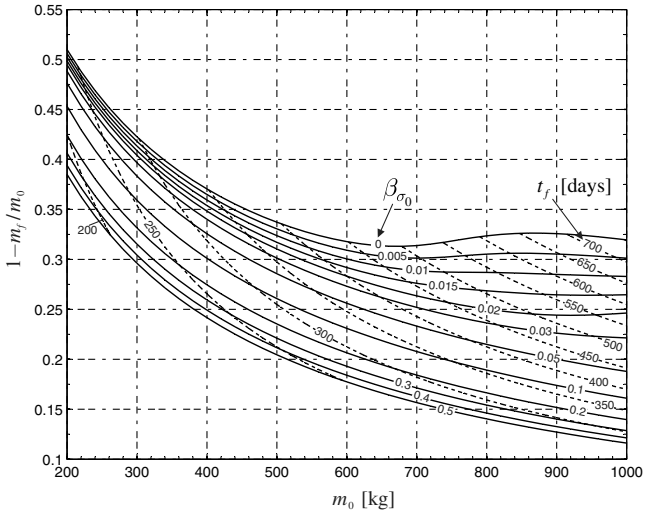

Fig. 1 Minimum-time ($\eta = 0$) Earth–Mars rendezvous trajectories.

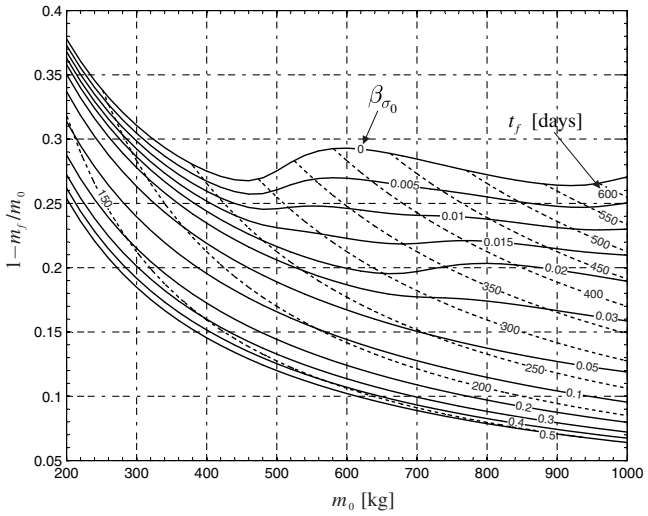

Fig. 2 Minimum-time ($\eta = 0$) Earth–Venus rendezvous trajectories.

because the optimal minimum-time trajectories are characterized by $P \equiv P_{\max}$ and $\tau = 1$ over all the mission time.

Figures 1 and 2 show a monotonic increase with β_{σ_0} in mission performance, both in terms of propellant consumption and flight time, due to the coupling of the SEP system with the solar sail. For example, assuming a total mass at launch $m_0 = 400$ kg (a value similar to that of SMART-1 spacecraft) a pure SEP-based spacecraft would be able to complete a Mars rendezvous in 348.8 days with a propellant consumption $m_p/m_0 = 0.37$. The corresponding trajectory is shown in Fig. 3, and the thrust angle time history is illustrated in Fig. 4 along with the spacecraft acceleration.

When this SEP system is coupled with a solar sail having an initial dimensionless sail loading $\beta_{\sigma_0} = 0.1686$ [corresponding to an ideal characteristic acceleration $a_c = 1$ mm/s^2, see Eq. (17)], the mission parameters experience a substantial variation with a reduction of 24% in both the propellant mass ($m_p/m_0 = 0.28$) and the mission time ($t_f = 264.7$ days) with respect to the pure electric propulsion case. The trajectory is shown in Fig. 5, and the thrust angle time history is illustrated in Fig. 6 along with the spacecraft acceleration. Note that the trajectory is characterized by a phase in which the sail produces no thrust (when the sail pitch angle is -90 deg). From Eq. (14), such a configuration requires a sizeable sail area $A \simeq 43,820$ m^2. For comparative purposes the Solar Polar Imager reference mission design [23,24] is based on a sailcraft with $A \simeq 19,200$ m^2, $m_0 = 450$ kg, and $a_c = 0.35$ mm/s^2.

Actually, the problem is more involved because, besides the increase in system complexity due to the solar sail, the presence of this additional thrust system involves, at the same time, an increase in the spacecraft dry mass, so that one may wonder whether there exists a benefit in terms of payload mass fraction deliverable. This problem will be discussed at the end of the paper.

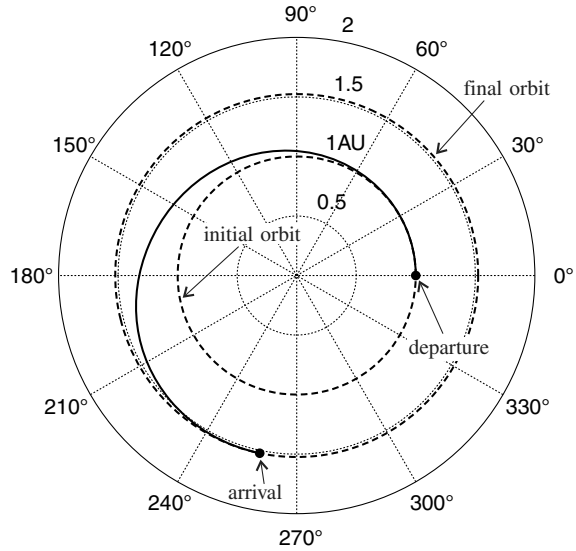

Fig. 3 Earth-Mars rendezvous trajectory with $m_0 = 400$ kg (pure SEP).

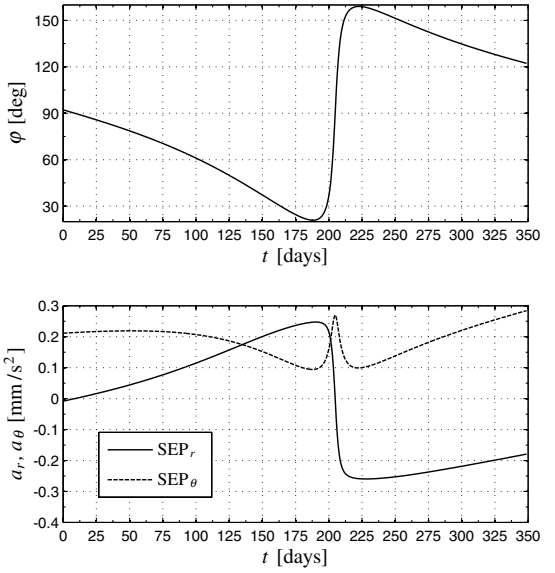

Fig. 4 Thrust angle and acceleration for an Earth–Mars rendezvous with $m_0 = 400$ kg (pure SEP).

Minimum Propellant Transfer

Another case of interest is that of minimum propellant rendezvous transfer. This corresponds to setting $\eta = 1$ in Eq. (20). Actually, this is a limit case because the propellant mass necessary to accomplish the mission is $m_p = 0$, independent of the spacecraft initial mass value. From a physical viewpoint, the reason for such a result is clear. In fact, the spacecraft has two propulsion systems that, by assumption, can be used independently, one from the other. Because the solar sail produces thrust without any propellant, the minimum propellant transfers correspond to those trajectories where the electric propulsion is never engaged, that is, $\tau = 0$ for all of the mission length. Of course, the use of a solar sail alone increases the total mission time when compared with a hybrid solution. For example, assuming $\beta_{\sigma_0} = 0.1686$, a mission to Mars with a solar sail alone needs a flight time $t_f = 448$ days, which is 70% greater than the minimum time corresponding to a hybrid solution with launch

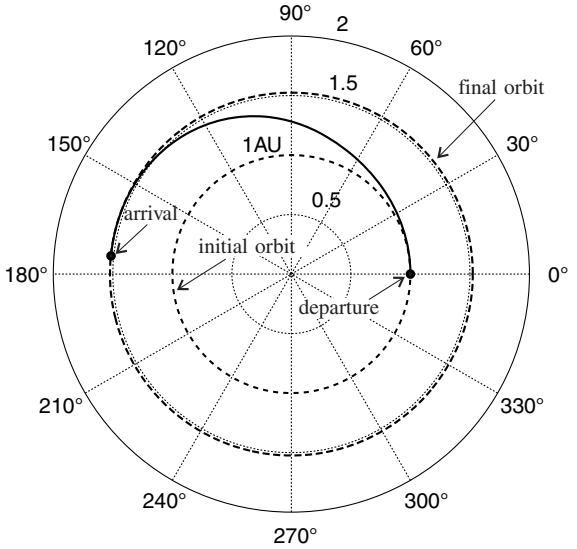

Fig. 5 Earth–Mars rendezvous trajectory with $m_0 = 400$ kg (HLTP case).

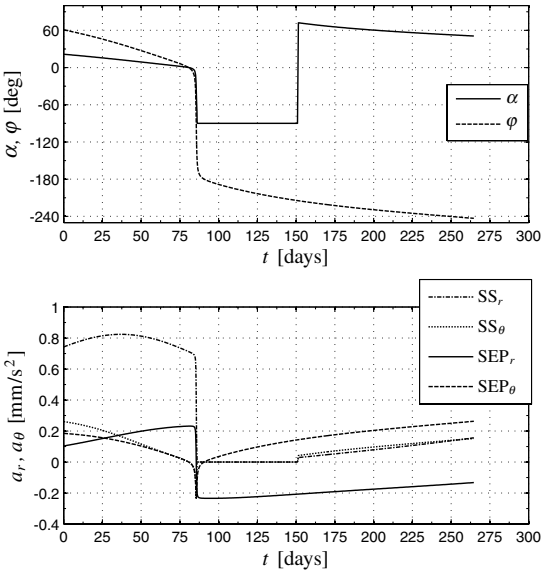

Fig. 6 Thrust angle and acceleration for an Earth–Mars rendezvous with $m_0 = 400$ kg (HLTP case).

mass $m_0 = 400$ kg. For an in-depth discussion of minimum-time rendezvous missions for solar sails with optical force model, the reader is referred to [16,18].

Tradeoff Between Propellant Mass and Flight Time

Having discussed the two limit cases of minimum time and minimum propellant transfers, it is now interesting to investigate the tradeoff solutions, where a given combination of flight time and propellant consumption is optimized according to the functional J in Eq. (20). In this analysis, the initial dimensionless sail loading is held constant and equal to $\beta_{\sigma_0} = 0.1686$, which corresponds to $a_c = 1$ mm/s^2. For a given value of the initial spacecraft mass, the tradeoff solutions are obtained by allowing η to range in the interval [0, 1]. Each combination (m_0, η) provides a different pair (m_f, t_f). The results for Earth–Mars and Earth–Venus missions have been summarized in Figs. 7 and 8.

These figures show that, m_0 being fixed, the propellant consumption decreases as long as the flight time increases (equivalently, as long as η is increased from zero to one). In the limit case $\eta = 1$, the curves provide the minimum trip times for a solar sail alone ($\tau = 0$ along the whole mission). The corresponding transfer

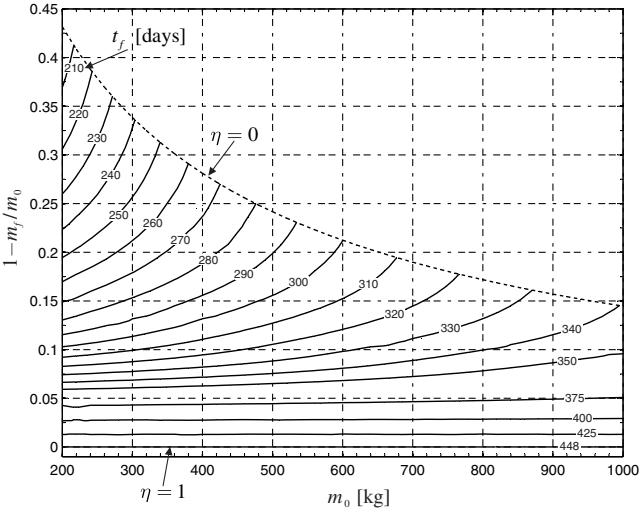

Fig. 7 Tradeoff for Earth–Mars rendezvous trajectories with $\beta_{\sigma_0} = 0.1686$ and $P_{\max} = 1.5$ kW.

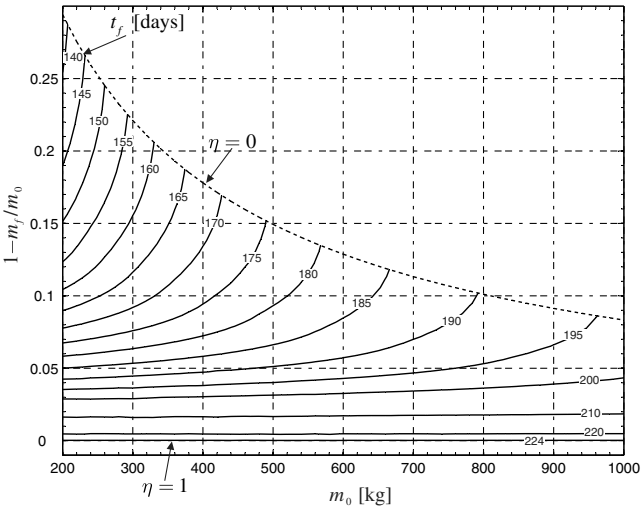

Fig. 8 Tradeoff for Earth–Venus rendezvous trajectories with $\beta_{\sigma_0} = 0.1686$ and $P_{\max} = 1.5$ kW.

times are in accordance to the values found in the literature for a solar sail spacecraft [16,18]. The graphs shown in Figs. 7 and 8 allow one to quickly gather information for preliminary mission studies and can be read in different ways. For example, consider an Earth–Mars mission for a spacecraft having $m_0 = 400$ kg. It is clear that a tradeoff between mission time and deliverable payload mass is possible. In fact, assuming a 10% increase in mission time with respect to $t_{\min}$ (that is, $t_f = 1.1 t_{\min} = 291.17$ days), the corresponding propellant consumption is $m_p/m_0 = 0.1525$, with a considerable decrease (−45.5%) with respect to the minimum-time case. The upper bound of each isocontour solution (dotted lines) obtained for a given value of mission time t_f coincides, as expected, with the minimum-time solutions ($t_f = t_{\min}, \eta = 0$) shown in Figs. 1 and 2 for the given value of β_{σ_0}. This means that while for a given initial spacecraft mass (m_0 is given) there exists a unique solution in terms of minimum transfer time (as well as a unique corresponding value of propellant consumption), for a given value of mission time t_f there exists a number of different spacecraft mass values that guarantee the same flight time. For example, Fig. 7 shows that, assuming $t_f = 300$ days, the corresponding mass values are in the range $m_0 \in [200, 600]$ kg and the dimensionless propellant consumption $(m_0 - m_f)/m_0 \in [0.10, 0.21]$. Therefore, the solution corresponding to a given value of m_0 [for example, $m_0 = 400$ kg and $(m_0 - m_f)/m_0 = 0.13$] can be "replaced" by another one (equivalent from the viewpoint of mission time) that needs less

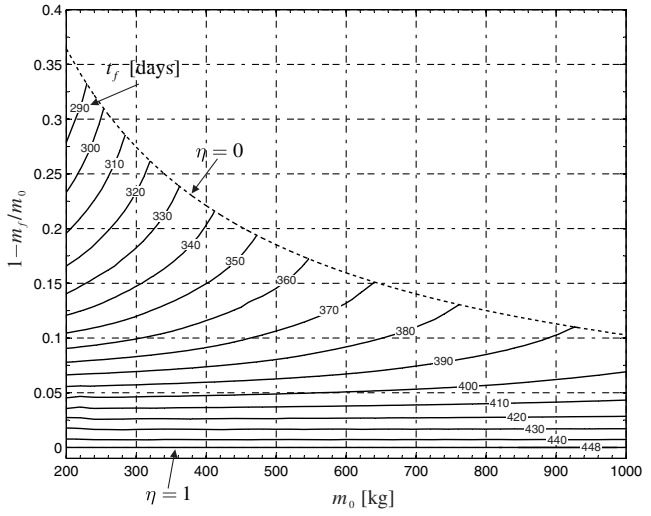

a) $P_{\max}$ = 0.46 kW

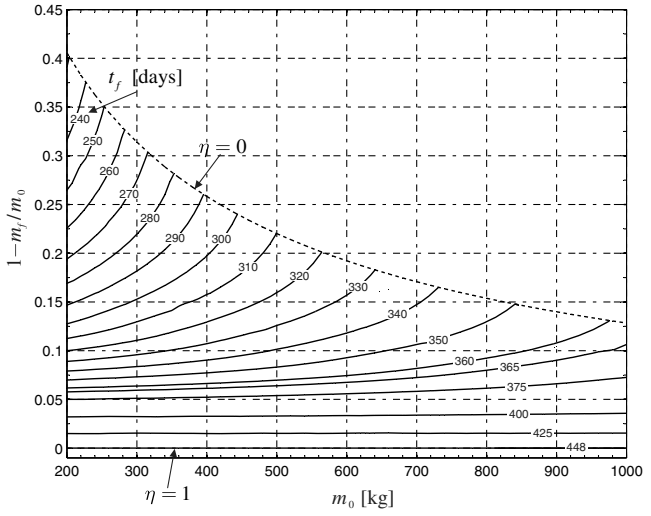

b) $P_{\max}$ = 1 kW

Fig. 9 Sensitivity of Earth–Mars trajectories ($\beta_{\sigma_0} = 0.1686$) to $P_{\max}$.

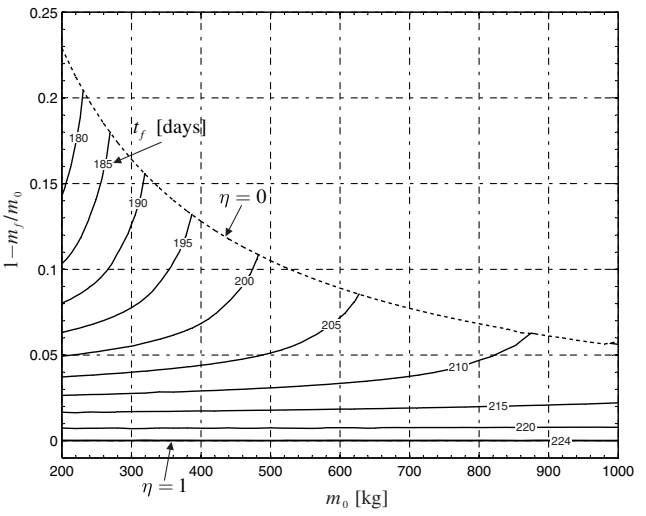

a) $P_{\max}$ = 0.46 kW

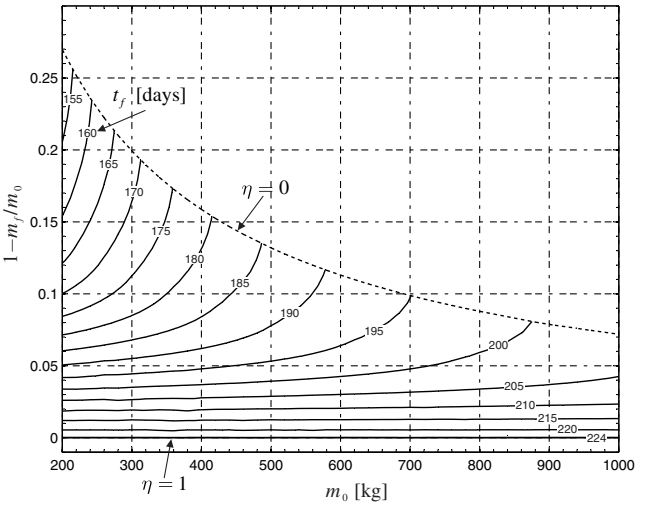

b) $P_{\max}$ = 1 kW

Fig. 10 Sensitivity of Earth–Venus trajectories ($\beta_{\sigma_0} = 0.1686$) to $P_{\max}$.

propellant but a smaller launch mass. This is exactly the possible tradeoff between mass and time.

Another case of practical interest consists in investigating the sensitivity of tradeoff solutions to $P_{\max}$. This amounts to studying the system performance when the input power is constrained within a maximum value different from the nominal value $P_{\max} = 1.5$ kW. The maximum input power value is an important parameter as it is closely connected to the power system mass and, therefore, to the spacecraft dry mass. At the same time, a decrease in $P_{\max}$ involves a considerable reduction in mission performance. This is clearly illustrated in Figs. 9 and 10 for missions towards Mars and Venus with $P_{\max} = (0.46, 1)$ kW.

For example, assuming a minimum-time ($\eta = 0$) Earth–Mars mission with $m_0 = 400$ kg and $\beta_{\sigma_0} = 0.1686$, the mission time is $t_f = 291$ days when $P_{\max} = 1$ kW, although $t_f = 337$ days when $P_{\max} = 0.46$ kW. These values correspond, respectively, to a mission time increase of 10% and 27% when compared with the nominal case $P_{\max} = 1.5$ kW.

Estimation of Payload Mass Fraction

As stated previously, a reasonable estimate of the payload mass fraction deliverable is necessary to obtain a realistic comparison between a pure electric and a hybrid system. To this end, we assume the following mass breakdown model for the spacecraft [1]

$$m_0 = m_e + m_{\text{pay}} + m_p + m_{\text{SS}} \tag{48}$$

where m_e is the mass of the SEP system, m_{SS} is the sail total mass, and m_{pay} is the sum of the payload mass and the mass of the remaining subsystems. From Eqs. (14) and (48) one has

$$h(m_0, \beta_{\sigma_0}, \sigma_{\text{SS}}) \triangleq \frac{m_e + m_{\text{pay}}}{m_0} = 1 - \frac{m_p}{m_0} - \beta_{\sigma_0} \frac{\sigma_{\text{SS}}}{\sigma^\star} \tag{49}$$

where $\sigma_{\text{SS}} \triangleq m_{\text{SS}}/A$ is the sail assembly loading, a parameter that is closely related to the value of the sail film areal density. Near-term demonstration missions are likely to have a σ_{SS} on the order of 25–30 g/m^2, even if midterm technology will probably allow values of 5–10 g/m^2. Future outer solar system missions will require an assembly loading on the order of 1 g/m^2.

Note that h, defined through Eq. (49), plays the role of a performance parameter, in that it allows one to quantify the impact of the solar sail on the whole system performance from the viewpoint of maximum deliverable payload. In fact, if $h_e \triangleq h(m_0, \beta_{\sigma_0} \equiv 0, \sigma_{\text{SS}})$ represents the performance parameter for a pure electric thruster, the hybrid solution is superior to the pure electric option as long as $h/h_e > 1$.

The performance increase of the hybrid solution with respect to the pure electric one is quantified in percentage terms in Fig. 11 for three different values of the sail assembly loading $\sigma_{\text{SS}} = (1, 3, 5)$. These results, valid for midhigh term solar sail technology, show significant improvements of HLTP over pure SEP systems and the promising performance of an hybrid configuration. Other simulations, not

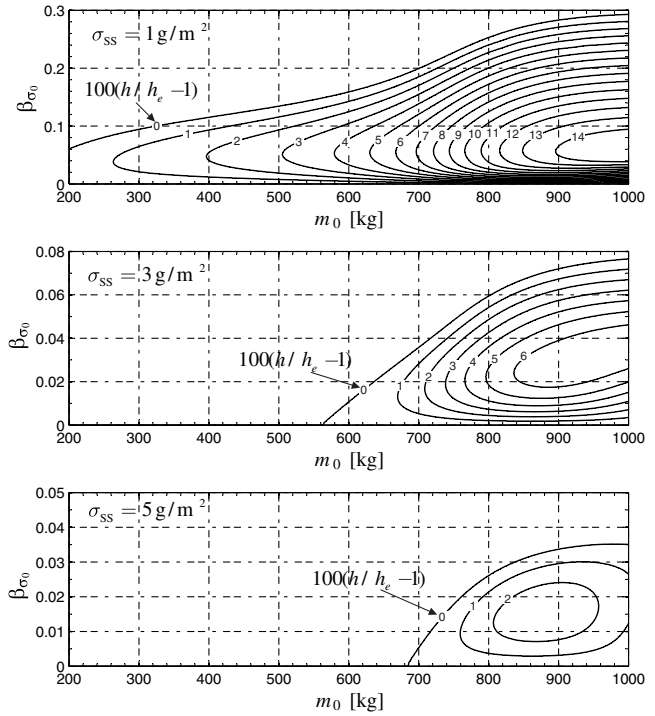

Fig. 11 Percent performance increase of hybrid over pure electric propulsion system.

shown here, reveal that if $m_0 \in [200, 1000]$ kg then $h/h_e < 1$ when $\sigma_{SS} > 6$. This implies that the hybrid solution tends to became less suitable for midhigh values of σ_{SS} because of the reduction in maximum deliverable payload.

Conclusions

We have investigated the performance of a hybrid low-thrust propulsion system, constituted by a solar electric thruster coupled with a solar sail. The solar sail may be seen as an auxiliary system capable of improving the mission performance. To quantify this effect on a rigorous basis, the problem has been formulated in terms of optimization of a scalar performance index that takes into account both the mission time and the propellant mass required to reach the target. A weighting parameter is used to trade between these two conflicting requirements. The problem is solved using an indirect approach and the resulting optimal control law is applied to circle-to-circle rendezvous transfers. The numerical examples show that tradeoff studies can be conducted with relative ease and with moderate computational effort. The simulation data have been collected in plots and graphs which are useful for preliminary mission analysis. They are of particular importance for allowing the designer to know exactly what technological level is required before a mission is feasible. Key features of the paper are the use of realistic models for both the solar electric thruster performance and the solar sail. In particular, the thrust and the propellant mass flow rate of the SEP system are modeled as a function of the total electric thruster input power using experimental data, whereas the solar sail behavior is described through an optical force model. A reasonable comparison between a hybrid and a conventional SEP system is made in terms of payload mass fraction deliverable for a given mission. Provided that high-performance solar sails are employed, the advantages of a hybrid configuration become remarkable.

References

[1] Brophy, J. R., "Advanced Ion Propulsion Systems for Affordable Deep-Space Missions," *Acta Astronautica*, Vol. 52, Nos. 2–6, Jan.–March 2003, pp. 309–316.

[2] Brophy, J. R., and Noca, M., "Electric Propulsion for Solar System Exploration," *Journal of Propulsion and Power*, Vol. 14, No. 5, Sept.–Oct. 1998, pp. 700–707.

[3] Dachwald, B., "Optimal Solar Sail Trajectories for Missions to the Outer Solar System," *Journal of Guidance, Control, and Dynamics*, Vol. 28, No. 6, Nov.–Dec. 2005, pp. 1187–1193.

[4] Leipold, M., Kassing, D., Eiden, M., and Herbeck, L., "Solar Sails for Space Exploration: The Development and Demonstration of Critical Technologies in Partnership," ESA Bulletin 98, June 1999.

[5] Montgomery, E. E., and Johnson, L., "Development of Solar Sail Propulsion for NASA Science Missions to the Inner Solar System," *45th AIAA/ASME/ASCE/AHS/ASC Structures, Structural Dynamics and Materials Conference*, AIAA Paper 2004-1506, 2004.

[6] Racca, G. D., "New Challenges to Trajectory Design by the Use of Electric Propulsion and Other New Means of Wandering in the Solar System," *Celestial Mechanics and Dynamical Astronomy*, Vol. 85, No. 1, 2003, pp. 1–24.

[7] Williams, S. N., and Coverstone-Carroll, V., "Benefits of Solar Electric Propulsion for the Next Generation of Planetary Exploration Missions," *Journal of the Astronautical Sciences*, Vol. 45, No. 2, April–June 1997, pp. 143–159.

[8] Schier, J., and Rush, J., "Space Communication Architecture Supporting Exploration and Science: Plans and Studies for 2010–2030," *1st Space Exploration Conference: Continuing the Voyage of Discovery*, AIAA Paper 2005-2517, 2005.

[9] Spurlock, D., "Space Exploration Systems Integration," *1st Space Exploration Conference: Continuing the Voyage of Discovery*, AIAA Paper 2005-2541, 2005.

[10] McNutt, R. L., "Solar System Exploration: A Vision for the Next Hundred Years," *55th International Astronautical Congress of the International Astronautical Federation, the International Academy of Astronautics, and the International Institute of Space Law*, International Astronautical Congress Paper 04-IAA.3.8.1.02, 2004.

[11] Mengali, G., and Quarta, A. A., "Trajectory Design with Hybrid Low-Thrust Propulsion System," *Journal of Guidance, Control, and Dynamics*, Vol. 30, No. 2, March–April 2007, pp. 419–426.

[12] Koppel, C. R., and Estublier, D., "SMART-1 Electric Propulsion Subsystem," *39th AIAA/ASME/SAE/ASEE Joint Propulsion Conference & Exhibit*, AIAA Paper 2003-4545, 2003.

[13] Milligan, D., Camino, O., and Gestal, D., "SMART-1 Electric Propulsion: An Operational Perspective," *9th International Conference on Space Operations*, AIAA Paper 2006-5767, 2006.

[14] Wright, J. L., *Space Sailing*, Gordon and Breach, Berlin, 1992, pp. 227–233.

[15] McInnes, C. R., *Solar Sailing: Technology, Dynamics and Mission Applications*, Springer–Praxis Series in Space Science and Technology, Springer–Verlag, Berlin, 1999, pp. 46–54.

[16] Mengali, G., and Quarta, A. A., "Optimal Three-Dimensional Interplanetary Rendezvous Using Nonideal Solar Sail," *Journal of Guidance, Control, and Dynamics*, Vol. 28, No. 1, Jan.–Feb. 2005, pp. 173–177.

[17] Leipold, M., and Götz, M., "Hybrid Photonic/Electric Propulsion," , Kayser-Threde, TR SOL4- TR-KTH-0001, Munich, Jan. 2002, ESA Contract No. 15334/01/NL/PA.

[18] Dachwald, B., Mengali, G., Quarta, A. A., and Macdonald, M., "Parametric Model and Optimal Control of Solar Sails with Optical Degradation," *Journal of Guidance, Control, and Dynamics*, Vol. 29, No. 5, Sept.–Oct. 2006, pp. 1170–1178.

[19] Bryson, A. E., and Ho, Y. C., *Applied Optimal Control*, Hemisphere, New York, 1975, Chap. 2, pp. 71–89.

[20] Lawden, D. F., *Optimal Trajectories for Space Navigation*, Butterworths, London, 1963, pp. 54–68.

[21] Stengel, R. F., *Optimal Control and Estimation*, Dover, New York, 1994, pp. 222–254.

[22] Alfano, S., and Thorne, J. D., "Circle-to-Circle Constant-Thrust Orbit Raising," *Journal of the Astronautical Sciences*, Vol. 42, No. 1, Jan.–March 1994, pp. 35–45.

[23] Dachwald, B., Ohndorf, A., and Wie, B., "Solar Sail Trajectory Optimization for the Solar Polar Imager (SPI) Mission," *AIAA/AAS Astrodynamics Specialist Conference and Exhibit*, AIAA Paper 2006-6177, 2006.

[24] Dachwald, B., and Wie, B., "Solar Sail Trajectory Optimization for Intercepting, Impacting, and Deflecting Near-Earth Asteroids," *AIAA Guidance, Navigation, and Control Conference and Exhibit*, AIAA Paper 2005-6176, 2005

B. Marchand
Associate Editor